NIH Public Access
Author Manuscript
*Biosens Bioelectron*. Author manuscript; available in PMC 2010 December 1.

Published in final edited form as:
*Biosens Bioelectron*. 2010 October 15; 26(2): 682–688. doi:10.1016/j.bios.2010.06.064.

# Highly sensitive and reusable Pt-black microfluidic electrodes for long-term electrochemical sensing

**Liangliang Qiang**[a], **Santhisagar Vaddiraju**[a,b], **James F. Rusling**[c,d], and **Fotios Papadimitrakopoulos**[a,c,*]

[a]Nanomaterials Optoelectronics Laboratory, Polymer Program, Institute of Materials Science, University of Connecticut, Storrs, CT 06269, United States

[b]Biorasis Inc., 23 Fellen Road, Storrs, CT 06268, United States

[c]Department of Chemistry, University of Connecticut, Storrs, CT 06269, United States

[d]Department of Cell Biology, University of Connecticut Health Center, Farmington, CT 06032, United States

## Abstract

Highly sensitive, long-term stable and reusable microfluidics electrodes have been fabricated and evaluated using $H_2O_2$ and hydroquinone as model analytes. These electrodes composed of a 300 nm Pt-black layer situated on a 5 μm thick electrodeposited Au layer, provide effective protection against electrooxidation of an underlying chromium adhesion layer. Using repeated cyclic voltammetric (CV) sweeps in flowing buffer solution, highly sensitive Pt-black working electrodes were realized with five- (four-) decade linear dynamic range for $H_2O_2$ (hydroquinone) and low detection limit of 10 nM for $H_2O_2$ and 100 nM for hydroquinone. Moreover, high sensitivity for $H_2O_2$ was demonstrated at low (0.3 V *vs*. Ag/AgCl) oxidation potentials, together with long-term stability and reusability for at least 30 days. Microfluidic flow was employed for desorption and reactivation of the nominally planar Pt-black electrodes. Such electrocatalytic surface architecture should be appropriate for long-term electrochemical detection of various molecules and biomolecules as well as in reusable immunoassay configurations.

### Keywords

Microfluidic; Hydrogen peroxide; Hydroquinone; Electrochemical activation; Biosensor; Limit of detection

## 1. Introduction

Microfluidic devices have attracted significant attention due to distinct advantages in numerous technological applications (Erickson and Li, 2004). This stems from decreases in volume of sample solutions and related reagents, small and portable size, low energy consumption and rapid manipulation of liquids, among other benefits (Squires and Quake, 2005; Whitesides, 2006). Consequently, an explosive growth in the use of microfluidic technology has occurred in devices designed for point-of-care diagnostics (Linder, 2007).

© 2010 Published by Elsevier B.V.

* Corresponding author at: University of Connecticut, Nanomaterials Optoelectronics Laboratory, Polymer Program, Institute of Materials Science, 97 N, Eagleville Road, U 3136, Storrs, CT 06269, United States. Tel.: +1 860 486 3447; fax: +1 860 486 4745. papadim@mail.ims.uconn.edu (F. Papadimitrakopoulos)..

NIH-PA Author Manuscript
NIH-PA Author Manuscript
NIH-PA Author Manuscript

NIH-PA Author Manuscript

NIH-PA Author Manuscript

NIH-PA Author Manuscript

The incorporation of microelectrochemical arrays into microfluidic devices enables further miniaturization and multiplexing, without compromising functionality (Bakker, 2004; Vaddiraju et al., 2010). To attain stable and continuous electrochemical measurements for lab-on-chip biosensor platforms the following requirements must be realized: (i) enable long-term electrochemical stability, (ii) high sensitivity, (iii) low detection limits, and (iv) long-term reusability or surface regeneration.

Planar electrochemical array architectures can be realized using standard lithographic techniques together with evaporation or sputtering of noble metal electrodes (e.g. gold, platinum, and palladium). In general, noble metal electrodes with sub-micron thickness are mechanically and electrochemically unstable for usage under high oxidation potential in contact with an electrolyte (Goss et al., 1991). For example, delamination, electrochemically-induced oxidation, and aging-induced cracking are among the main culprits for mechanical electrode failure, while catalytic poisoning and surface fouling reduce device sensitivity (Goss et al., 1991; Ling et al., 2003).

A variety of metabolic and immunoassay based electrochemical sensing methods involves the detection of $H_2O_2$ or small molecular weight (MW) mediators (Bakker, 2004; Tipnis et al., 2007; Vaddiraju et al., 2009, 2010; Warsinke et al., 2000; Yu et al., 2006). Along with signal amplification, highly sensitive, stable and reliable electrode geometries are typically needed in order to measure low concentrations of the analyte of interest (Kim and Oh, 1996; Kim et al., 2007). Sensitivity of biosensor electrodes can be attained by the use of high-surface area electrodes made from nanomaterials including single- and multi-walled carbon nanotubes (Kim et al., 2007; Rusling et al., 2009a,b; Yu et al. 2006), nanoparticles, nanorods, or nanowires of noble metals (Hrapovic et al., 2004; Mani et al., 2009), and conductive polymers (Ekanayake et al., 2007; Karyakin et al., 2009). Transferring such nanostructured geometries from individual electrodes (e.g. single disk electrode) to planar arrays housed within microfluidic channels present a number of challenges with respect to adhesion, repeatability, device complexity and cost. The ease of fabrication of Au-based electrodes together with the high catalytic activity of activated Pt overcoats provide a viable approach to address these challenges (Chen et al., 2002; De Corcuera et al., 2005). A number of reports indicate that micro- and nanostructured Pt, in the form Pt-black (De Corcuera et al., 2005), Pt-micropost-arrays (Ren et al., 2009), Pt-alloys and mesoporous Pt (Evans et al., 2002) provide a significant increase in both surface area and catalytic activity towards redox reactions of $H_2O_2$ and small molecule mediators. However, retention of catalytic activity and the subsequent reusability of these nanostructured electrodes remains problematic.

In this paper, we report methodology to fabricate highly sensitive, stable and reusable Au/Pt-black electrodes in planar array configuration for glass-supported microfluidic devices. Using repeated cyclic voltammetric (CV) activation by sweeps from −0.5 to +0.9 V vs. Ag/AgCl, sensitivity was increased by two orders of magnitude compared to non-activated electrodes. The nanostructured array electrodes retain high sensitivity at continuous bias for more than 8 h at applied potentials as high as +0.7 V vs. Ag/AgCl. Using daily reactivation with repeated CV sweeps, stable and reproducible operation was achieved in excess of 30 days. These electrodes exhibit a five-decade linear dynamic range for $H_2O_2$ detection and a four-decade linear dynamic range for hydro-quinone and detection limits in the low nM range. To the best of our knowledge, this is the first microfluidic electrode array geometry that enables enhanced sensitivity, together with reproducibility, reusability, and prolonged operation.

NIH-PA Author Manuscript
NIH-PA Author Manuscript
NIH-PA Author Manuscript



## 2. Experimental

### 2.1. Materials and instruments

All chemicals were procured from Aldrich. Gold and chromium (99.99%) were obtained for Kurt Lesker. The glass substrates were Fisherfinest premium plain glass microscope slides. Shipley S1813 photoresist and Developer-351 were purchased from Microchem Corp., Newton, MA. Gold plating solution (Orotemp 24 RTU RACK) was obtained from Technic Inc., Anaheim, CA. Scanning electron microscopic (SEM) images were collected by JEOL JSM-6335F with a cold cathode field emission source at 10.0 kV and working distance of 14.4 mm.

### 2.2. Chip fabrication

All microfluidic chips (Fig. 1) were constructed on glass substrates using standard 300 nm UV photolithography (Price et al., 2009), using a Karl Süss MA-6 mask aligner. Glass substrates (1 in. × 1.5 in.) were cleaned by sonicating in soap water, acetone, and deionized (DI) water for 30 min in each step. These substrates were then spin coated with 1.2 μm of photoresist film followed by baking (120 °C, 10 min) Following UV exposure, development and plasma cleaning, a 10 nm chromium/100 nm gold layer was evaporated and lifted off (in acetone) to afford electrode patterning (Fig. 1b). Subsequently, following an 8 h vacuum treatment in hexamethyldisilazane (HMDS) vapors, a 2 μm thick positive photoresist was deposited and patterned to create coarse openings over all electrodes and contact pads. One hour of exposure in a gold plating solution (10 $\mu Amm^{-2}$ current density) enabled the electroplating of 5 μm thick Au over the exposed gold electrodes. Subsequently, the entire device was rinsed in acetone to remove all photoresist, and re-spun coated with 2 μm of a final positive photoresist to define the final electroactive area of electrodes (with a circular opening of 900 μm in diameter) and 2 mm × 5 mm rectangular windows for contact pads. Working and counter electrodes were realized by electrodepositing 300 nm of platinum in 10 mM $H_2PtCl_6$ and 0.1 M HCl at 12 $\mu Amm^{-2}$ for 15 min (De Corcuera et al., 2005). A pseudo-reference electrode was made by electrodepositing silver from an aqueous solution of AgI (0.17 M), KI (2.4 M) (to form a water-soluble silver complex) together with $CaAc_2$ (0.4 M) at 12 $\mu Amm^{-2}$ for 15 min and oxidized in 0.1 M of HCl solution (Mousey et al., 1993;Tipnis et al., 2007). The final structure of the working electrode is shown in Fig. 1d. The configuration of working, counter and reference electrodes is shown in Fig. 1a.

### 2.3. Amperometric experiments

All electrochemical experiments were carried out in a microfluidic geometries defined by the glass substrate (that supports all electrodes) and a poly(dimethylsiloxane) (PDMS) block with a 1.5 mm × 22 mm × 50 μm (in width, length, thickness) microchannel, fabricated as reported previously (McDonald and Whitesides, 2002). Two access holes were punched using a 23-gauge needle and connected to 0.28 mm polyethylene (PE) tubing (Fig. 1a). Flow in the microfluidic channel was achieved by withdrawing fluid from a vial across the channel using a pump-operated syringe. Out of eight electrodes, the first, fourth and fifth dots on the chips were employed as working, reference and counter electrodes, respectively. A CHI 1010A electrochemical workstation was used to collect all electrochemical data presented herein. Before amperometric testing, the working electrode was conditioned by cyclic voltammetric sweeps (21 cycles in range −0.5 to +0.9 V at a rate of 100 mV/s) in flowing phosphate buffer saline (PBS, pH = 7.4) (30 μL/min). The activation step was employed once per day for an entire day's experiments. After a stable background current was reached, amperometric traces were obtained by adding the desired concentration of $H_2O_2$ (or hydroquinone) solution into 20 mL of PBS under constant stirring.

NIH-PA Author Manuscript

NIH-PA Author Manuscript

NIH-PA Author Manuscript

# 3. Results and discussion

## 3.1. Electrode fabrication

Standard UV photolithography was employed to pattern gold electrodes onto glass substrates (Laschi and Mascini, 2006). The need to increase adhesion between glass and gold necessitates the use of an adhesive layer that typically comprises of a thin (10–20 nm) Cr or Ti layer (Laschi and Mascini, 2006). Unfortunately, the inherent electrochemical reactivity and corrosion-prone nature of Cr or Ti at high oxidation potentials, that in the first place enables these electrodes to firmly adhere to hydrophilic surfaces (*i.e*. glass, $SiO_2$-coated Si), presents a major problem (Ling et al., 2003). For example, electrodes with 10 nm of Cr and 100 nm of Au (Fig. 1b and e) can be easily delaminated after several cyclic voltammetric scans (−0.5 to +0.8 V *vs*. Ag/AgCl, 100 mV/s) (Fig. 1c and f). The gray-bluish area in Fig. 1e depicts the intact Cr adhesion layer (corresponding to Fig. 1b), when imaged from the backside. Following the 21 cycles of the aforementioned voltammetric sweeps, the appearance of gold rim and gold spots becomes apparent (Fig. 1f). These correspond to a partly dissolved Cr layer (as shown in Fig. 1c) that exposes the gold from the overlaying Au electrode at edges and pinholes (Fig. 1c). Substantial removal of the Cr adhesion layer results in the electrode delamination. The onset of electrode delamination typically takes place within an hour of applying continuous +0.7 V bias *vs*. Ag/AgCl, and eventually leads to a complete destruction of the electrochemical device within few hours.

In order to improve the stability of the gold electrodes, a thick overlayer thick Au was electroplated to completely seal all pinholes (Fig. 1d). 5 μm of electrodeposited Au was found to yield greater stability than 1 and 3 μm thick films. Similar electrode-position of a thick layer of Pt from aqueous solutions of $H_2PtCl_6$ was found corrosive to the underlying adhesion Cr layer and was not pursued further. Subsequently, a 2 μm thick positive photoresist was patterned to cover the edges of the electrodes and protect them against sideways attack (Fig. 1d). This electrode configuration could be operated extensively at relatively high oxidation potentials (*i.e*. +0.8 V) or conditioned by CV sweeps from−0.5 to +0.9 V with no significant corrosion or electrode-delamination.

A thin layer (300 nm) of Pt-black was electrodeposited onto the planar gold electrodes. This is accomplished by electroplating an aqueous solution of $H_2PtCl_6$ (10 mM) in HCl (0.1 M) that yields a nanostructured surface composed of Pt-nanoparticles that range from 10 to 100 nm (Fig. 1g) (De Corcuera et al., 2005;Hrapovic et al., 2004). The electrocatalytic activity of Pt-black electrodes has been reported to vary substantially (Chakraborty and Retna Raj, 2009;De Corcuera et al., 2005;Evans et al., 2002). Typically, an optimization of electroplating current, potential and precursor concentration is needed to attain high sensitivity (De Corcuera et al., 2005). Pt-black electrodes usually loose their sensitivity within few days of storage, which inevitably degrades long-term device reliability. In order to address this problem, we have developed a combination of thick Pt-black layer followed by an activation step, using multiple cyclic voltammetric (CV) sweeps.

Unlike the previously employed less than 1 min Pt-black electrodeposition (Baldwin et al., 2002; Ling et al., 2003), a longer electroplating time was used to afford a 300 nm Pt-black layer. This longer electrodeposition time enables the complete coverage of the underlying Au electrode with Pt-black, a necessary step to prevent high potential (above 0.8 V) induced Au dissolution that leads to Pt-black delamination. This provides additional stability to the Pt-black during the CV activation sweeps from −0.5 to +0.9 V *vs*. Ag/AgCl, a potential where Pt begins to dissolve (Tang et al., 2010).

Fig. 2a shows the amperometric current *vs*. $H_2O_2$ concentration in 30 μL/min PBS flow for different working electrode surfaces at 0.4 V *vs*. Ag/AgCl. The slopes of these curves

NIH-PA Author Manuscript

NIH-PA Author Manuscript

NIH-PA Author Manuscript

represent the sensitivity for $H_2O_2$ detection. The sensitivity of the freshly deposited Pt-black electrodes increased from 0.092 nA $\mu M^{-1}$ $mm^{-2}$ of the bare gold electrode to 0.65 nA $\mu M^{-1}$ $mm^{-2}$. Following activation by 21 sequential sweeps from−0.5 to +0.9 V, at 100 mV/s, the sensitivity of the Pt-black electrodes increases by 33 times vs. that of freshly deposited Pt electrodes, to a value of 22 nA $\mu M^{-1}$ $mm^{-2}$. This value is 240-fold larger than that for the Au electrodes alone.

To the best our knowledge, although CV-based electrode conditioning is typically employed with stand alone working electrodes, it was never before used for lithographically patterned planar array electrodes due to their poor adhesion stabilities at both Au/Cr/glass and Au/Pt-black interfaces (Baldwin et al., 2002; Goss et al., 1991; Ling et al., 2003). This improvement may be due to flow-induced removal of various adsorbed residues on the Pt-black surfaces, along with the selective oxidation of Pt atoms that promote the formation of selected crystallographic planes (Hall et al., 2000; Kim and Oh, 1996). The latter is shown in Fig. 2b, where the respective area under the hydrogen adsorption/desorption curve increases 2–3-fold after the CV-activation step. The CV-activation step increases the surface area of Pt-black and exposes two sets of CV peaks that have been assigned to hydrogen adsorption/desorption on Pt(1 1 0) (−0.25 V) and Pt(1 0 0) (−0.15 V) due to preferred etching of other planes (Armand and Clavilier, 1987a,b; Clavilier et al., 1986; Kim and Oh, 1996).

### 3.2. Hydrogen peroxide detection

The ubiquitous nature of $H_2O_2$ as the byproduct of oxidase enzyme reactions renders it a good choice for bioanalyte detection (Bakker, 2004; Tipnis et al., 2007; Vaddiraju et al., 2009, 2010; Wang, 2008). The sensitivity of the CV-activated Pt-black electrodes was investigated as a function of oxidation potential, flow rate, concentration of $H_2O_2$, and sensor stability (Fig. 3). First, the amperometric response for continuous steps in peroxide concentration (not flow injection) was investigated in order to determine the optimum operational potential. Four $H_2O_2$ concentrations (10, 20, 30, 40 μM) at 50 μL/min PBS flow rate were used to test the sensor with at least 3 repetitive experiments and sensitivity was estimated by linear regression. Relative standard deviations (RSD) for all data are less than 5% except for the data in Fig. 3a which had an RSD of 28% (when tested at 100 mV) and 9% (when tested at 200 mV). Fig. 3a illustrates the sensitivity, background, and signal-to-noise (S/N) ratio of these sensors as a function of applied potential *vs*. Ag/AgCl. The extreme catalytic activity of these CV-activated Pt-black electrodes provides excellent sensitivity at potentials as low as 0.2 V. Since these sensors are operated in the presence of oxygen, residual oxygen reduction provides a high background signal at low oxidation potential (*i.e*. lower than 0.25 V). Here the background current was collected in the absence of $H_2O_2$ by biasing the sensor for 200 s and recording the mean average of last 10 s recorded. These sensors afforded the largest S/N ratio for $H_2O_2$ detection at 0.3 V with a sensitivity of 25.3 ± 0.2 nA $\mu M^{-1}$ $mm^{-2}$. A somewhat higher sensitivity of 27.0 ± 0.4 nA $\mu M^{-1}$ $mm^{-2}$ was obtained at 0.5 V, which slightly decreases at 0.6 and 0.7 V.

Since Faradaic current in any electrochemical reaction of a dissolved species is controlled by the mass transport rate of reactants to the respective electrode surface, the dependence of sensitivity *vs*. flow rate within the microfluidic channel was investigated. As shown in Fig. 3b, the sensitivity was found to asymptotically increase for higher flow rates. The sensitivity at 200 μL/min (41 ± 2nA $\mu M^{-1}$ $mm^{-2}$) is four times higher than 5 μL/min (10.9 ± 0.1 nA $\mu M^{-1}$ $mm^{-2}$) at 0.5 V *vs*. Ag/AgCl. Since this increase is more pronounced at higher flow rates, the intermediate value of 50 μL/min was chosen for the remainder of the experiments, unless otherwise noted.

Fig. 3c illustrates the linear dynamic range for CV-activated Pt-black electrodes as a function of $H_2O_2$ concentration at 0.3 V *vs*. Ag/AgCl. Five decades linearity was observed

NIH-PA Author Manuscript

NIH-PA Author Manuscript

NIH-PA Author Manuscript

with the lowest detection limit by concentration-step amperometry of 10 nM. The inset in Fig. 3c illustrates the amperometric current vs. time at the limit of detection (*i.e*. 0.17 nA for 10 nM of $H_2O_2$) which is three times that of the noise (*ca*. 0.05 nA). Additional improvements in sensitivity (down to 1 nM of $H_2O_2$) might be obtained by using flow injection configuration and possibly by minimizing noise-induced coupling stemming from environment such as high amperage circuits, labor pump-induced vibrations (Trojanowicz, 2009;Xu et al., 2005).

Table 1 illustrates the comparison of sensitivity, limit of detection (LOD), linear range and operational potential for $H_2O_2$ detection for various Pt-based electrochemical configuration and testing method (*i.e*. concentration-step *vs*. flow injection amperometry) against our CV-activated, Pt-black electrode. Most of the electrodes reported in literature operate around 0.5–0.6 V in Table 1. Our sensors can be operated at potential as low as 0.2 V, and more optimally at 0.3 V, presents the highest sensitivity reported so far, better than Pt-decorated single walled carbon nanotube (SWCNT) reported recently, which operated at 0.55 V (Hrapovic et al., 2004). Taking into account that flow injection method provides *ca*. an order of magnitude better performance (Xu et al., 2005), both dynamic range and LOD of our CV-activated Pt-black electrode is comparable to the Nano-Pt structures supported on glassy carbon electrodes (Chakraborty and Retna Raj, 2009). Moreover, it should also be noted that flow injection is not applicable for *in vivo* continuous monitoring of metabolites such as $H_2O_2$, glucose and lactate, which can be a major thrust for such device architecture.

### 3.3. Hydroquinone (HQ) detection

HQ is a typical substrate and mediator in horseradish peroxidase (HRP) labeled immunoassays (Rusling et al., 2009a,b). Fig. 4 illustrates the linear dynamic range for CV-activated Pt-black electrodes as a function of HQ concentration at 0.5 V *vs*. Ag/AgCl and 50 μL/min flow of PBS. Four decades linearity was observed with the lowest detection limit (under continuous polarization) of *ca*. 100 nM and sensitivity of 7.1 nA $\mu M^{-1}$ $mm^{-2}$. The one order of magnitude decrease in the limit of detection (LOD) between HQ (100 nM) and $H_2O_2$ (10 nM) is believed to originate from HQ's substantial higher molecular weight and size, which greatly impede its diffusion to nanostructured surface of Pt-black (Park et al., 2003). This also affects HQ sensitivity, which is ca. 4 times lowers than that $H_2O_2$. For planar electrodes the ratio of amperometric current for $H_2O_2$ and HQ typically scales to the two third power of their ratio of diffusion coefficients (Elbicki et al., 1984). With experimentally determined diffusion coefficients of $1.43 \times 10^{-9}$ and $0.89 \times 10^{-9}$ $m^2$ $s^{-1}$ for $H_2O_2$ and HQ (Van Stroe-Biezen et al., 1993), respectively at 25 °C in PBS buffer, the observed sensitivity ratio of $H_2O_2$ and HQ is 2.7 times greater than the predicted ratio for planar smooth electrodes. Such increase is believed to originate from the nanostructured surface of our Pt-black working electrode that is more in favor of small molecules like $H_2O_2$ (Park et al., 2003).

### 3.4. Repeatability and long-term stability

Following the aforementioned CV sweep activation of the Pt-black working electrodes in 50 μL/min PBS, we observed minimal decay of sensitivity for the remainder of electrochemical experiments on the same day. However, when the electrodes were dried, the sensitivity decreased by *ca*. 20% overnight upon exposure to air at room temperature. However, when these electrodes were subjected, before operation, to a second CV sweep-activation of Pt-black, they recovered the initial activity (*i.e*. 26.5 ± 0.6 nA $\mu M^{-1}$ $mm^{-2}$ at 0.5 V *vs*. Ag/AgCl). Fig. 3d illustrates a long-term (30 day) sensitivity study of these sensors against $H_2O_2$ detection under continuous bias at 0.5 V and 50 μL/min flow of PBS. The overall 30-day average sensitivity of 26.6 ± 0.5 nA $\mu M^{-1}$ $mm^{-2}$ is identical to that recorded in the first day's experiment, indicative of the robust sensor design that enables repeated Pt-black

NIH-PA Author Manuscript

NIH-PA Author Manuscript

NIH-PA Author Manuscript

reactivation steps with no physical damage to the underlying electrode structure. Moreover, electrode to electrode reproducibility within the same microfluidic chip is greater than 95% between electrodes within the same chip and within 90% between electrodes of different chips.

### 3.5. Poisoning and reactivation of Pt-black

Surface poisoning of electrodes is a major concern for all electroanalytical methods (Duwensee et al., 2009). This often originates from adsorption of ions, organic molecules, proteins, or polymers onto the electrode surface, which can passivate or deactivate catalytic sites responsible for redox activity (Hubbard, 1990; Vaddiraju et al., 2010). Aromatic amines, such as o-phenylenediamine (o-PD), have been shown to bind strongly on various metal electrode surfaces (Hubbard, 1990), and if exposed to high enough oxidative potential (above 0.4 V *vs*. Ag/AgCl), they electrodeposit as conjugated oligomers or polymers (Garjonyte and Malinauskas, 1999). Fig. 5 illustrates a model study for o-PD-poisoning of activated Pt-black electrodes. Following a number of controlled exposure experiments to 10 mM of aqueous solutions of o-PD, the electrodes were rinsed with PBS and tested at 0.3 V *vs*. Ag/AgCl (below the electropolymerization voltage of o-PD to poly(o-PD)) under 50 μL/min flow of PBS. The sensitivity of the original, Pt-black activated electrode (Fig. 5a) decreased by 60% (Fig. 5b) upon one hour soak in o-PD solution without any applied bias. Following the aforementioned CV-activation step (from −0.5 to +0.9 V) in flowing PBS (50 μL/min flow), the sensitivity recovered to 99.2% of the original (Fig. 5c). Knowing that o-PD polymerizes above 0.4 V and the CV activation sweep exposes the working electrode to up +0.9 V, this provides a first indication that the PBS flow is capable of carrying away higher molecular weight (MW) oligomers of o-PD within the applied potential range. When this electrode was exposed again to o-PD solution (Fig. 5d) and CV-activated in still (not flowing) PBS solution (Fig. 5e), a further decrease was recorded, down to 16% of the original sensitivity. This suggests that CV activation also causes oligomerization of o-PD, and if the surrounding PBS solution is not moving to carry away the high MW byproducts, it leads to greater poisoning, presumably by deposition of the oligomers onto the electrode. Conducting another CV-activation step in flowing PBS (50 μL/min flow) can partially remove the o-PD oligomers and recover up to 85% of the original sensitivity (Fig. 5f). This provides an explicit indication of the importance of the mobile phase to carry away residues stripped away by the CV sweep.

## 4. Conclusions

The data presented above support the successful fabrication and characterization of highly sensitive, reusable, microfabricated electrode arrays with long-term stability in microfluidic configurations. Stability and performance relies on a 5 μm thick, electrodeposited Au electrode that provides effective protection against electrooxidation of the chromium adhesion underlayer. With the help of a 300 nm thick electrodeposited Pt-black layer activated by multiple cyclic voltammetric (CV) sweeps in flowing PBS solution once daily, highly sensitive array devices were realized, with 4 to 5 orders of magnitude linear dynamic range and low nM detection limits for $H_2O_2$ and hydroquinone. Moreover, a high sensitivity for $H_2O_2$ was demonstrated for low (0.3 V) oxidative potentials, together with at least 30 days stability and reusability. The flow of PBS in microfluidics arrangement was critical for contaminant desorption and reactivation of these planar Pt-black electrodes. Such microfluidic electrochemical architecture, due to their inherent flow convection, it represents a viable platform for long-term metabolic biosensors and reusable immunoassay configurations. Future experiments will focus on testing the stability of these electrodes to harsh environments (temperature, pH, *etc*.) as well as establishing their applicability to immunoassays and metabolic biosensors.

NIH-PA Author Manuscript

NIH-PA Author Manuscript

NIH-PA Author Manuscript

## Acknowledgments

Financial support for this study was obtained from NIH ES013557, NIH/NHLBI 1-R21-HL090458-01, Telemedicine and Advanced Technology Research Center (TATRC) at the U.S. Army Medical Research and Material Command (USAMRMC) (Award No. W81XWH-09-1-0711) AFOSR FA9550-09-1-02-1 and National Institute of Biomedical Imaging & Bioengineering award (R43EB011886). The authors would like to thank Dr. L. Zhang and Dr. J. Wang for helping with SEM characterization.

## References

Armand D, Clavilier J. J. Electroanal. Chem 1987a;225:205–214.

Armand D, Clavilier J. J. Electroanal. Chem 1987b;233:251–265.

Bakker E. Anal. Chem 2004;76:3285–3298. [PubMed: 15193109]

Baldwin RP, Roussel TJ Jr. Crain MM, Bathlagunda V, Jackson DJ, Gullapalli J, Conklin JA, Pai R, Naber JF, Walsh KM, Keynton RS. Anal. Chem 2002;74:3690–3697. [PubMed: 12175155]

Chakraborty S, Retna Raj C. Biosens. Bioelectron 2009;24:3264–3268. [PubMed: 19442506]

Chen X, Matsumoto N, Hu Y, Wilson GS. Anal. Chem 2002;74:368–372. [PubMed: 11811410]

Clavilier J, Armand D, Sun SG, Petit M. J. Electroanal. Chem 1986;205:267–277.

De Corcuera JIR, Cavalieri RP, Powers JR. J. Electroanal. Chem 2005;575:229–241.

Duwensee H, Vazquez-Alvarez T, Flechsig GU, Wang J. Talanta 2009;77:1757–1760. [PubMed: 19159794]

Ekanayake EMIM, Preethichandra DMG, Kaneto K. Biosens. Bioelectron 2007;23:107–113. [PubMed: 17475472]

Elbicki JM, Morgan DM, Weber SG. Anal. Chem 1984;56:978–985. [PubMed: 6742436]

Erickson D, Li D. Anal. Chim. Acta 2004;507:11–26.

Evans SAG, Elliott JM, Andrews LM, Bartlett PN, Doyle PJ, Denuault G. Anal. Chem 2002;74:1322–1326. [PubMed: 11924592]

Garjonyte R, Malinauskas A. Sens. Actuators B 1999;56:85–92.

Goss CA, Charych DH, Majda M. Anal. Chem 1991;63:85–88.

Hall SB, Khudaish EA, Hart AL. Electrochim. Acta 2000;45:3573–3579.

Hrapovic S, Liu Y, Male KB, Luong JHT. Anal. Chem 2004;76:1083–1088. [PubMed: 14961742]

Hubbard AT. Langmuir 1990;6:97–105.

Karam P, Halaoui LI. Anal. Chem 2008;80:5441–5448. [PubMed: 18543955]

Karyakin AA, Kuritsyna EA, Karyakina EE, Sukhanov VL. Electrochim. Acta 2009;54:5048–5052.

Kim CS, Oh SM. Electrochim. Acta 1996;41:2433–2439.

Kim SN, Rusling JF, Papadimitrakopoulos F. Adv. Mater 2007;19:3214–3228. [PubMed: 18846263]

Laschi S, Mascini M. Med. Eng. Phys 2006;28:934–943. [PubMed: 16822696]

Linder V. Analyst 2007;132:1186–1192. [PubMed: 18318278]

Ling TGI, Beck M, Bunk R, Forsen E, Tegenfeldt JO, Zakharov AA, Montelius L. Microelectron. Eng 2003;67–68:887–892.

Mani V, Chikkaveeraiah BV, Patel V, Gutkind JS, Rusling JF. ACS Nano 2009;3:585–594. [PubMed: 19216571]

McDonald JC, Whitesides GM. Acc. Chem. Res 2002;35:491–499. [PubMed: 12118988]

Mousey F, Harrison DJ, O'Brien DW, Rajotte RV. Anal. Chem 1993;65:2072–2077. [PubMed: 8372970]

Park S, Chung TD, Kim HC. Anal. Chem 2003;75:3046–3049. [PubMed: 12964749]

Price DT, Rahman ARA, Bhansali S. Biosens. Bioelectron 2009;24:2071–2076. [PubMed: 19101134]

Ren HX, Huang XJ, Kim JH, Choi YK, Gu N. Talanta 2009;78:1371–1377. [PubMed: 19362203]

Rusling JF, Sotzing G, Papadimitrakopoulosa F. Bioelectrochemistry 2009a;76:189–194. [PubMed: 19403342]

Rusling, JF.; Yu, X.; Munge, BS.; Kim, SN.; Papadimitrakopoulos, F. Engineering the bioelectronic interface: applications to analyte biosensing and protein detection.. In: Davis, JJ., editor.

NIH-PA Author Manuscript

NIH-PA Author Manuscript

NIH-PA Author Manuscript

Engineering the Bioelectronic Interface. Royal Society of Chemistry; UK: 2009b. p. 94-118.ISBN: 0854041656, 9780854041657

Squires TM, Quake SR. Rev. Mod. Phys 2005;77:977–1026.

Tang L, Han B, Persson K, Friesen C, He T, Sieradzki K, Ceder G. J. Am. Chem. Soc 2010;132:596–600. [PubMed: 20017546]

Tipnis R, Vaddiraju S, Jain F, Burgess DJ, Papadimitrakopoulos F. J. Diabetes Sci. Technol 2007;1:193–200. [PubMed: 19888406]

Trojanowicz M. Anal. Chim. Acta 2009;653:36–58. [PubMed: 19800474]

Vaddiraju S, Burgess DJ, Jain FC, Papadimitrakopoulos F. Biosens. Bioelectron 2009;24:1557–1562. [PubMed: 18823767]

Vaddiraju S, Tomazos I, Burgess DJ, Jain FC, Papadimitrakopoulos F. Biosens. Bioelectron 2010;25:1553–1565. [PubMed: 20042326]

Van Stroe-Biezen SAM, Everaerts FM, Janssen LJJ, Tacken RA. Anal. Chim. Acta 1993;273:553–560.

Wang J. Chem. Rev 2008;108:814–825. [PubMed: 18154363]

Warsinke A, Benkert A, Scheller FW. Fresenius' J. Anal. Chem 2000;366:622–634. [PubMed: 11225774]

Whitesides GM. Nature 2006;442:368–373. [PubMed: 16871203]

Xu W, Sandford RC, Worsfold P, Carlton A, Hanrahan G. Crit. Rev. Anal. Chem 2005;35:237–246.

Yang M, Qu F, Lu Y, He Y, Shen G, Yu R. Biomaterials 2006;27:5944–5950. [PubMed: 16945408]

You T, Niwa O, Tomita M, Hirono S. Anal. Chem 2003;75:2080–2085. [PubMed: 12720344]

Yu X, Munge B, Patel V, Jensen G, Bhirde A, Gong JD, Kim SN, Gillespie J, Gutkind JS, Papadimitrakopoulos F, Rusling JF. J. Am. Chem. Soc 2006;128:11199–11205. [PubMed: 16925438]

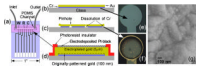

**Fig. 1.**

Schematic layout of (a) patterned electrodes together with PDMS microfluidics channel. (b) Microlithographically defined Cr/Au electrode without the side-edge protection and thick gold before and (c) after application of positive bias on electrodes described in (b) that dissolves the underlying Cr adhesion layer causing the formation of pinholes and edge delamination. (d) Cross-section design of Pt-black electrodes, that are resistant to delamination as a result of side-edge protection via a photoresist insulator, and the removal of pinholes by the growth of a thick (5 μm) electroplated gold layer. Optical images of electrodes described in (b) (viewed from the back side) showing the gray layer of Cr before (e) and after (f) 21 cycles of CV from −0.5 to 0.8 V vs. Ag/AgCl, which causes partial Cr dissolution and exposes the gold over layer at the edges and pinholes. (g) SEM image of the top surface of CV-activated Pt-black electrode.



NIH-PA Author Manuscript NIH-PA Author Manuscript NIH-PA Author Manuscript

NIH-PA Author Manuscript
NIH-PA Author Manuscript
NIH-PA Author Manuscript



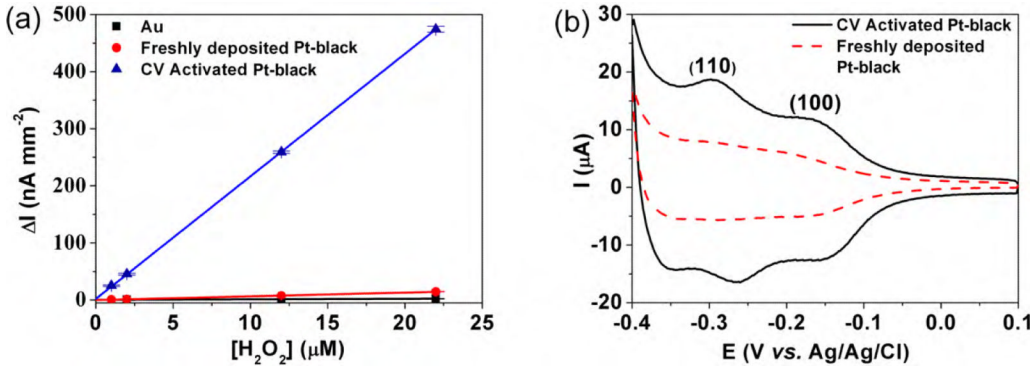


**Fig. 2.**

(a) Influence of $H_2O_2$ concentration on amperometric current for bare Au, freshly electrodeposited Pt-black and CV-activated Pt-black electrodes, at 0.4 V *vs*. Ag/AgCl with 30 μL/min PBS flow. (b) Cyclic voltammograms of freshly deposited and CV-activated Pt-black electrodes in 0.5 M $H_2SO_4$ at 50 mV/s.

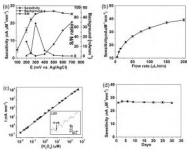

**Fig. 3.**

(a) $H_2O_2$ sensitivity vs. potential of CV-activated Pt-black electrodes, along with corresponding background current (in the absence of $H_2O_2$) and signal-to-noise (background) (S/N) ratio. (b) $H_2O_2$ sensitivity versus flow rate (at 0.5 V *vs*. Ag/AgCl). (c) Linear dynamic range ($y = 46.7 + 23.1x$, $R^2 = 0.995$) for $H_2O_2$ detection at 0.3 V *vs*. Ag/AgCl, 50 μL/min PBS flow. Inset show staircase amperometric curve for four additions of 10 nM $H_2O_2$ at limit of detection (LOD), indicated by the respective four steps. (d) Long-term reproducibility study of sensitivity of these sensors against $H_2O_2$ detection, following daily CV-reactivation.



NIH-PA Author Manuscript NIH-PA Author Manuscript NIH-PA Author Manuscript

NIH-PA Author Manuscript

NIH-PA Author Manuscript

NIH-PA Author Manuscript

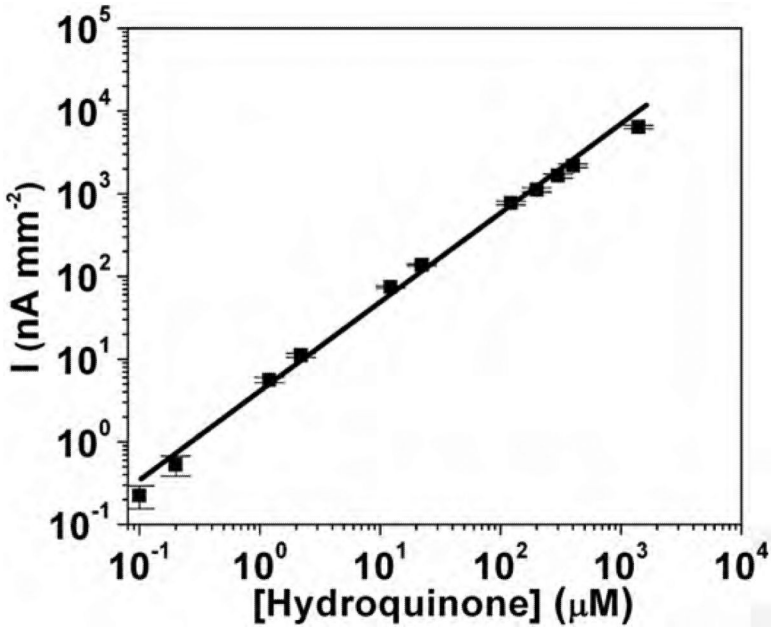


**Fig. 4.**

Linear dynamic range ($y = 114.9 + 7.14x$, $R^2 = 0.995$) for hydroquinone detection by CV-activated Pt-black electrodes operated at 0.5 V *vs*. Ag/AgCl and 50 μL/min PBS flow.

NIH-PA Author Manuscript

NIH-PA Author Manuscript

NIH-PA Author Manuscript

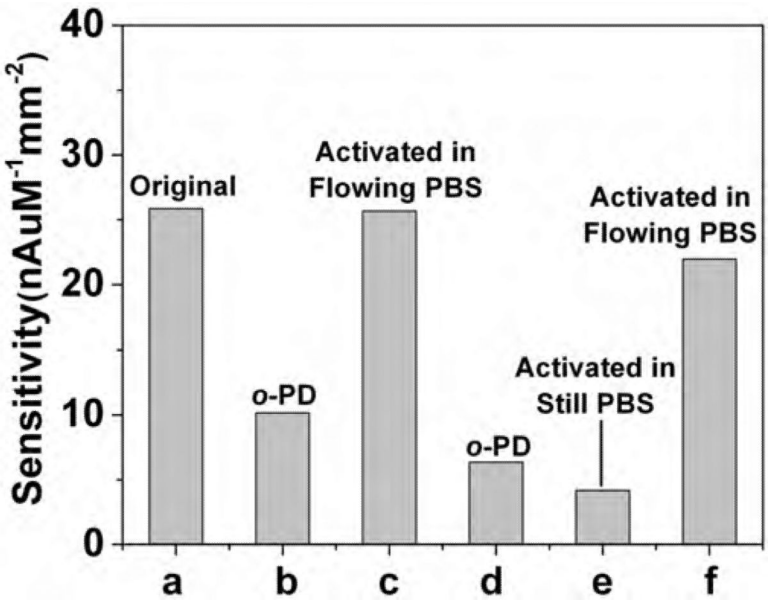


**Fig. 5.**

Poisoning and CV (−0.5 to 0.9 V *vs*. Ag/AgCl, 100 mV/s) reactivation study showing sensitivities of the: (a) original CV-activated Pt-black electrode; (b) following 1 h. immersion in 10 mM aqueous o-phenylenediamine (o-PD); (c) after CV-reactivation in flowing PBS (50 μL/min); (d) after re-immersion in o-PD solution; (e) after CV-activated in a still (not flowing) PBS solution; and (f) after CV-activation again in flowing PBS solution (50 μL/min).

NIH-PA Author Manuscript NIH-PA Author Manuscript NIH-PA Author Manuscript



**Table 1**

Comparison of key electrochemical parameters for electrochemical $H_2O_2$ sensing using various Pt-decorated electrodes.

| Electrode | Detection potential (V) | Linear range | LOD (nM) | Sensitivity ($AM^{-1}$ $cm^{-2}$) | Testing method | Ref. |
|---|---|---|---|---|---|---|
| SWCNT/Pt | 0.55[a] | 25 nM–10 μM | 25 | 3.57 | C.A. | Hrapovic et al. (2004) |
| Mesoporous Pt | 0.6[b] | 0.02–100 mM | 4500 | 2.8 | C.A. | Evans et al. (2002) |
| Pt Nanowire | 0[b] | 100 nM–60 mM | 50 | 0.54 | C.A. | Yang et al. (2006) |
| Pt-NEGCF | 0.6[a] | 500 nM–2 mM | 7.5 | 0.055 | F.I.A. | You et al. (2003) |
| Nano-Pt | 0.5[a] | 0.5 nM–4 mM | 0.5 | 0.15[c] | F.I.A. | Chakraborty and Retna Raj (2009) |
| PDDA/Pt NP | 0.6[a] | 42 nM–0.16 mM | 42 | 1 | C.A. | Karam and Halaoui (2008) |
| CV-activated Pt-Black | 0.3[a] | 10 nM–0.3 mM | 10 | 4.08[d] | C.A. | This work |

[a] *vs.* Ag/AgCl.

[b] *vs.* SCE.

[c] Estimated from Fig. 2 in Chakraborty and Retna Raj (2009).

[d] At flow rate of 0.2 ml/min; (C.A.) concentration-step amperometry. (F.I.A.) flow injection analysis; (SWCNT/Pt) Pt-decorated single walled carbon nanotubes; (Pt-NEGCF) Pt-nanoparticles embedded in glassy carbon film; (PDDA/Pt NP) Pt-nanoparticles adhered in poly(diallyldimethyl ammonium chloride).

*Biosens Bioelectron*. Author manuscript; available in PMC 2010 December 1.